The interstellar medium and the massive stellar content towards the SNR G18.1−0.1 and neighbouring H II regions

S. Paron,[1,2,3]★† W. Weidmann,[4]† M. E. Ortega,[1] J. F. Albacete Colombo[5] and A. Pichel[1]

[1]*Instituto de Astronomía y Física del Espacio (CONICET-UBA), CC 67, Suc. 28, 1428 Buenos Aires, Argentina*
[2]*FADU, Universidad de Buenos Aires, Ciudad Universitaria, Buenos Aires, Argentina*
[3]*CBC, Universidad de Buenos Aires, Ciudad Universitaria, Buenos Aires, Argentina*
[4]*Observatorio Astronómico Córdoba, Universidad Nacional de Córdoba, Argentina*
[5]*Centro Regional Zona Atlántica (CURZA), Universidad Nacional del Comahue, Viedma, Argentina*

ABSTRACT

We perform a multiwavelength study of the SNR G18.1−0.1 and nearby several H II regions (infrared dust bubbles N21 and N22, and the H II regions G018.149−00.283 and G18.197−00.181). Our goal is to provide observational evidence supporting the view that massive stars are usually born in clusters from the same molecular cloud, which then produce, along their evolution, different neighbouring objects such as H II regions, interstellar bubbles and supernova remnants (SNRs). We suggest that the objects analysed in this work belong to a same complex located at the distance of about 4 kpc. Using molecular data we inspected the interstellar medium towards this complex and from optical and X-ray observations we looked for OB-type stars in the region. Analysing public ^{13}CO $J = 1$–0 data we found several molecular structures very likely related to the H II region/SNR complex. We suggest that the molecular gas is very likely being swept and shaped by the expansion of the H II regions. From spectroscopic optical observations obtained with the 2.15-m telescope at CASLEO, Argentina, we discovered three O-type stars very likely exciting the bubbles N21 and N22, and an uncatalogued H II region northwards of bubble N22, respectively. Also we found four B0-5 stars, one towards the bubble N22 and the others within the H II region G18.149−0.283. By inspecting the *Chandra* Source Catalogue we found two-point X-ray sources and suggest that one of them is an early O-type star. Finally, we inspected the large-scale interstellar medium around this region. We discovered a big molecular shell of about 70×28 pc in which the analysed complex appears to be located in its southern border.

Key words: stars: massive – ISM: clouds – H II regions – ISM: supernova remnants.

1 INTRODUCTION

Nowadays, it is well known that massive stars in our Galaxy are born predominantly within the dense cores of giant molecular clouds (for a thorough discussion of the star formation theories, see McKee & Ostriker 2007). They usually form and evolve in clusters, hence it is expectable to observe several H II regions in different evolutionary stages and probably also supernova remnants (SNRs) in a same Galactic neighbourhood. Some examples of this spatial coincidence are the field towards W28, with several SNRs and H II regions (e.g.

Nicholas et al. 2011), the SNR W44 and the H II region G034.8−0.7 (Paron et al. 2009; Ortega et al. 2010), the luminous blue variable (LBV) star candidate G24.73+0.69, some H II regions and the SNR G24.7+0.6 (Petriella, Giacani & Paron 2011; Petriella, Paron & Giacani 2012). Moreover, large amounts of molecular gas in the surroundings of H II regions and SNRs are usually observed. The shock and ionization fronts from these objects, which compress and sweep up the molecular gas, can trigger the formation of a new generation of massive stars. This has been extensively probed towards the borders of H II regions (e.g. Deharveng, Zavagno & Caplan 2005; Pomarès et al. 2009; Brand et al. 2011) where processes such as 'collect and collapse' (Elmegreen & Lada 1977) and/or radiative driven implosion (Lefloch & Lazareff 1994, 1995) can be taking place.

The goal of this work is to provide observational evidence supporting that massive stars are usually born in clusters from material of the same molecular cloud, which then produce, along their

★ E-mail: sparon@iafe.uba.ar
† Visiting Astronomer, Complejo Astronómico El Leoncito operated under agreement between the Consejo Nacional de Investigaciones Científicas y Técnicas de la República Argentina and the National Universities of La Plata, Córdoba and San Juan.

evolution, neighbouring H II regions, interstellar bubbles and SNRs that can interact with the parental cloud. To perform this we select a very rich region in which lie the SNR G18.1−0.1 and several H II regions, two of them catalogued as infrared dust bubbles by Churchwell et al. (2006). In Section 2, we describe the studied H II region/SNR complex; Section 3 presents an analysis of the interstellar medium (ISM) around these sources; in Section 4 we present an optical spectroscopic search for OB-type stars (the H II regions exciting star candidates) and an analysis of two X-ray point sources; Section 5 presents a larger scale ISM study around the complex, and finally Section 6 summarizes the obtained results.

2 THE STUDIED H II REGION/SNR COMPLEX

In Fig. 1 we present the 22×22 arcmin^2 region where the H II region/SNR complex lies in a colour composite image as seen in the *Spitzer*-IRAC 8 μm emission (blue), the radio continuum emission at 20 cm (red) and the *Spitzer*-MIPSGAL emission at 24 μm (green). We used the mosaicked image from the Galactic Legacy Infrared Mid-Plane Survey Extraordinaire (GLIMPSE) in the *Spitzer*-IRAC band at 8 μm which has an angular resolution of ∼1.9 arcsec (see Benjamin et al. 2003). MIPSGAL is a survey of the same region as GLIMPSE, using MIPS instrument (24 and 70 μm) on *Spitzer* (Carey et al. 2009). The MIPSGAL resolution at 24 μm is 6 arcsec. The radio continuum data at 20 cm, with a full width at half-maximum synthesized beam of about 5 arcsec, was extracted from the New GPS of the Multi-Array Galactic Plane Imaging Survey (Helfand et al. 2006) which was conducted using the Very Large Array (VLA). In what follows we describe each object based on the information that appears in the literature.
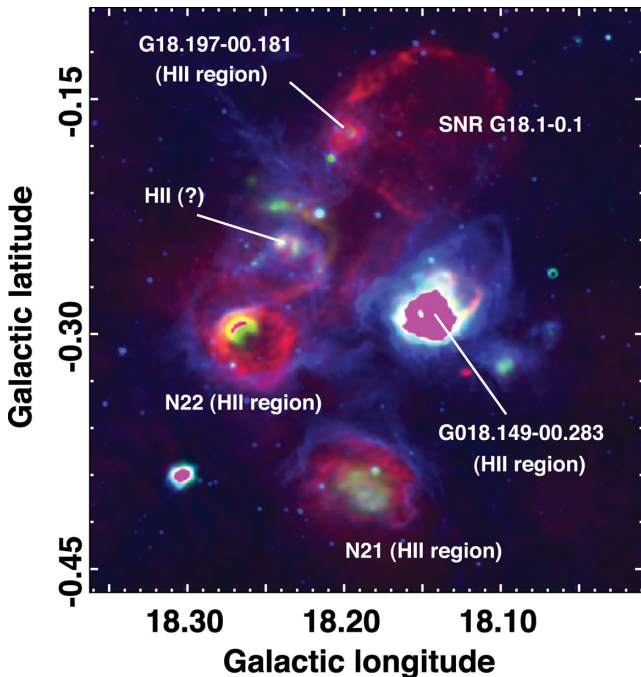
Figure 1. The studied region presented in a three-colour image. The radio continuum emission at 20 cm is displayed in red, the IRAC-*Spitzer* 8 μm emission in blue and the MIPS-*Spitzer* 24 μm emission in green. The objects analysed in this work are indicated. The arc feature in N22 and almost the whole interior of G18.149−0.283 are saturated in 24 μm.

2.1 SNR G18.1−0.1

SNR G18.1−0.1 or G18.16−0.16 (Green 2009) is a poor studied SNR that was first observed at 57.5 MHz by Odegard (1986), who identified it as SNR G18.1−0.2. The author also mentions the presence of the source Sharpless 2−53 (Sharpless 1959), which is related to the H II regions complex composed by N21, N22 and G018.149−00.283 as can be seen in Fig. 1. Based on the distance estimated for the H II regions complex of 4.5 kpc (Downes et al. 1980), Odegard (1986) suggests this value as the minimum kinematic distance for the SNR. Later, the SNR G18.1−0.1 was associated with the X-ray source AXJ182435−1311, which was observed with *ASCA* (Sugizaki et al. 2001). More recently, this shell SNR was identified in the VLA survey of the Galactic plane at 90 cm by Brogan et al. (2006), reporting fluxes of 7.6, 3.9 and 3.0 Jy at 90, 20 and 11 cm, respectively. They derived a spectral index of $\alpha = -0.5 \, (S_\nu \propto \nu^\alpha)$ using the emission at 90 and 20 cm, and $\alpha = -0.4$ using the 90 and 11 cm data.

2.2 Infrared dust bubbles N21 and N22

Churchwell et al. (2006, 2007) using GLIMPSE data, catalogued almost 600 infrared dust bubbles: full or partial rings bordered by a photodissociation region (PDR), seen mainly at 8 μm, which usually encloses ionized gas and hot dust observed at 24 μm. Most of these bubbles are H II regions as is the case of bubbles N21 and N22 displayed in Fig. 1. The bubble N22, G18.259−0.307 H II region (Kolpak et al. 2003), has a recombination line velocity of $v_{\mathrm{LSR}} \sim 51 \, \mathrm{km \, s^{-1}}$, and is located at ∼4.1 kpc. The ISM around N22 was very recently investigated by Ji et al. (2012), finding some evidence of triggered star formation. The bubble N21 is not catalogued in Kolpak et al. (2003) but it appears as the H II region G018.20−00.40 in Lockman (1989) with a systemic velocity of $v_{\mathrm{LSR}} \sim 43.2 \, \mathrm{km \, s^{-1}}$. The spectral resolutions in Kolpak et al. (2003) and Lockman (1989) are $2.5 \, \mathrm{km \, s^{-1}}$ and between 2 and $4 \, \mathrm{km \, s^{-1}}$, respectively.

Watson et al. (2008) identified 21 young stellar object candidates around N21, and based on a spectral energy distribution fitting to numerical hot stellar photosphere models, they suggested some stars to be the possible exciting sources of this H II region. According to Anderson & Bania (2009), who analysed a sample of 291 Galactic H II regions with the aim of resolving the distance ambiguity, N21 is related to the source called C18.19−0.40 with a resolved distance $d = 3.6$ kpc, and N22 to C18.26−0.30 with $d = 4.0$ kpc.

2.3 H II region G018.149−00.283

H II region G018.149−00.283 is not catalogued as an infrared dust bubble and, according to Kolpak et al. (2003), has a recombination line velocity of $v_{\mathrm{LSR}} \sim 53.9 \, \mathrm{km \, s^{-1}}$ and is located at the distance of ∼4.1 kpc. This is in agreement with the distance catalogued for U18.15−0.28, the source related to this H II region in Anderson & Bania (2009).

2.4 H II region G18.197−00.181

The source that is superimposed over the eastern border of the SNR is the H II region G18.197−00.181 (Lockman 1989), which has a systemic velocity $v_{\mathrm{LSR}} \sim 46.1 \, \mathrm{km \, s^{-1}}$. This H II region is related to C18.20−0.18 in Anderson & Bania (2009), whose distance ($d = 3.7$ or 12.4 kpc) is not resolved because it presents a discrepancy between the used methods to resolve the ambiguity.

2.5 H II region (?)

In Fig. 1, based on the morphology of the IR and radio continuum emission, we indicated another possible H II region (it appears with an interrogation mark in the figure), which was not found in any catalogue. This source has a PDR visible in the 8 μm band, which encloses ionized gas observed at 20 cm and hot dust observed at 24 μm, typical characteristics of H II regions (see e.g. Povich et al. 2007; Watson et al. 2008; Everett & Churchwell 2010). In this case two peaks at 24 μm appear, one towards the centre and the other almost in a border of this possible H II region. According to the coordinates, this object should be H II region G18.237−0.240.

In order to summarize, Table 1 presents the sources, their Galactic coordinates, the radius in the case of the SNR, the average radius for the H II regions and the linear sizes. The SNR radius was extracted from Green (2009), while the average radius of bub-

Table 1. Analysed sources.

Source	l	b	Radius (arcmin)	Linear size (pc)
SNR G18.1−0.1	18°.147	−0°.169	8.0	9.3
G18.197−00.181	18°.197	−0°.181	0.5	0.6
G018.149−00.283	18°.149	−0°.283	1.6	1.8
N21	18°.190	−0°.396	2.2	2.5
N22	18°.254	−0°.305	1.7	1.9
H II(?)	18°.237	−0°.240	0.5	0.6

bles N21 and N22 from Churchwell et al. (2006). In the case of G018.149−00.283, G18.197−00.181 and the possible unknown H II region, the average radius was estimated as was done by Churchwell et al. (2006) for the infrared dust bubbles. The linear size is the spatial diameter of the sources by assuming a distance of 4 kpc.

3 THE INTERSTELLAR MEDIUM

Anderson et al. (2009) analysed individually the molecular content towards a sample of 301 Galactic H II regions, which contains the H II regions studied in this work. Using the same molecular data base we analyse the molecular material towards the whole SNR/H II region complex in order to have a complete picture of the relation between the molecular gas and the complex. The data were extracted from the Galactic Ring Survey (GRS) which was performed by the Boston University and the Five College Radio Astronomy Observatory. The survey maps the Galactic Ring in the ^{13}CO $J = 1$–0 line with an angular and spectral resolution of 46 arcsec and 0.2 km s^{-1}, respectively (see Jackson et al. 2006). The observations were performed in both position-switching and On-The-Fly mapping modes, achieving an angular sampling of 22 arcsec.

By inspecting the whole ^{13}CO $J = 1$–0 data cube towards the H II region/SNR complex we find several molecular structures very likely related to the sources within the velocity range that goes from 40 to 57 km s^{-1}. Fig. 2 displays the integrated velocity channel maps of the ^{13}CO $J = 1$–0 emission every ∼1 km s^{-1} shown in grey. The
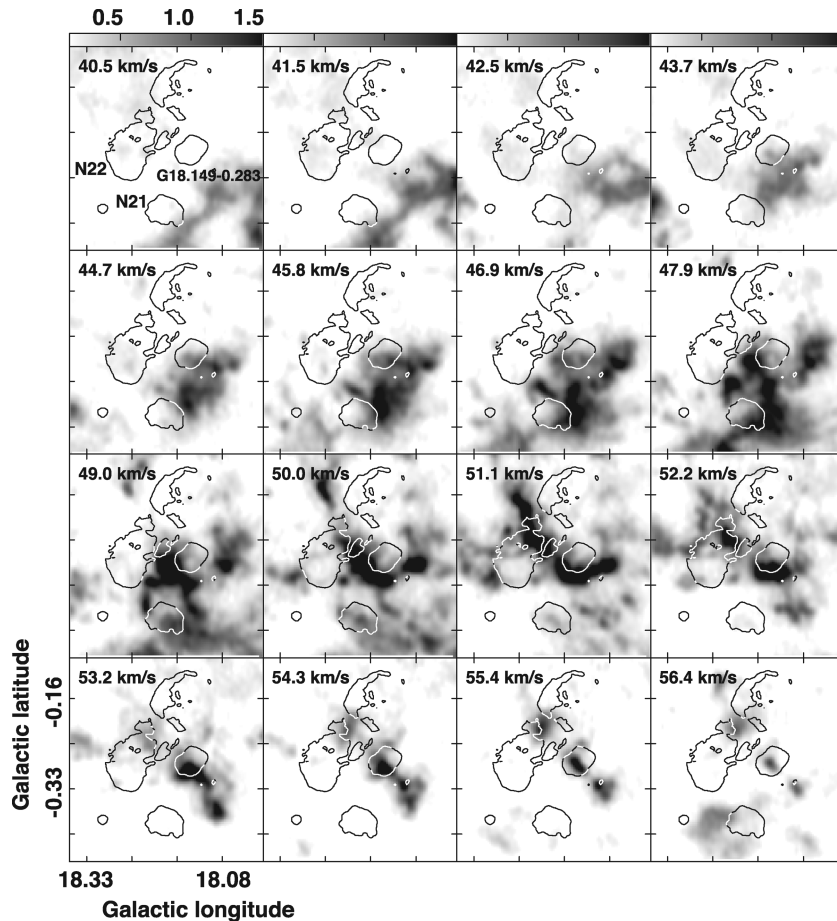
Figure 2. Integrated velocity channel maps of the ^{13}CO $J = 1$–0 emission (in grey) every ∼1 km s^{-1}. The grey-scale is displayed at the top of the figure and is in K km s^{-1}. The contours are the smoothed radio continuum emission. The H II region G18.149−0.283 and bubbles N21 and N22 are indicated in the first panel.

contours are the smoothed radio continuum emission, which are included just to mark the sources' position. For a better localization of them, in the first panel, the H II region G18.149−0.283 and bubbles N21 and N22 are indicated. The molecular gas is mostly distributed in the surroundings of bubbles N21, N22 and G18.149−0.283, appearing in the interstices between them, which indicates that it is very likely being swept and shaped by their expansion. It can be seen that N21 ($v_{LSR} \sim 43\,km\,s^{-1}$) is surrounded by molecular gas mainly in the velocity range 42.6–52.4 km s^{-1}, the N22 bubble ($v_{LSR} \sim 51\,km\,s^{-1}$) has likely associated molecular gas between 47.9 and 54.3 km s^{-1} (for a deeper analysis of the ISM around this bubble, see Ji et al. 2012), and in the velocity range that goes from 45.8 to 56.4 km s^{-1} appears gas likely related to G018.149−00.283 ($v_{LSR} \sim 54\,km\,s^{-1}$). Concerning to the SNR and the H II region G18.197−00.181, it can be noticed that some molecular gas appears towards the SNR eastern and southern borders. This can be better observed in Fig. 3, which shows the contours of the ^{13}CO $J = 1$–0 emission integrated from 39 to 59 km s^{-1} over the radio continuum at 20 cm and the IR at 8 μm emissions. It is noticeable how the lower ^{13}CO $J = 1$–0 contour surrounds the southeastern borders of the SNR and H II region G18.197-00.181, suggesting a relation between these objects and the molecular gas. Moreover, some molecular gas appears entering into the SNR radio continuum shell, precisely towards the south of the H II region G18.197−00.181 where the radio continuum emission is weaker.

The velocity range in which the molecular gas appears very likely related to the complex is in agreement with the catalogued systemic velocities of the H II regions. From the Galactic rotation model of Fich, Blitz & Stark (1989), this velocity range gives the near distance interval of about 3.6–4.5 kpc and the farthest distance range of about 11.8–12.7 kpc. The near distance interval is in agreement with the distances catalogued in Anderson & Bania (2009). Moreover, taking into account that the detection rate for IR dust bubbles in GLIMPSE peaks at the distance of 4.2 kpc within a horizon of
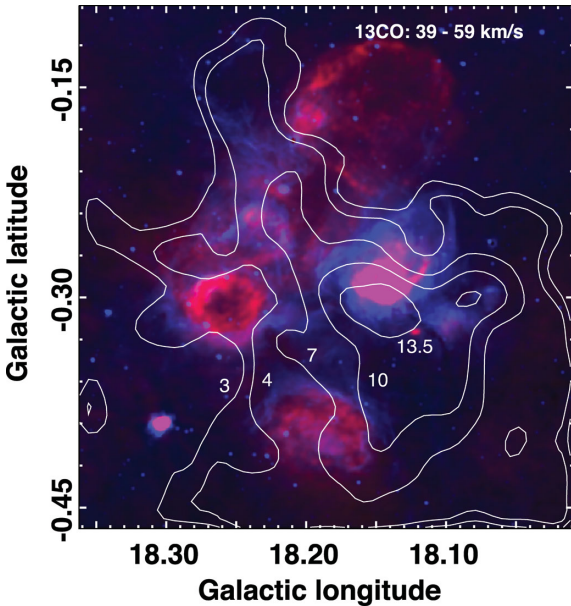
Figure 3. Two-colour image with the radio continuum emission at 20 cm displayed in red and the IRAC-*Spitzer* 8 μm emission in blue. The white contours are the ^{13}CO $J = 1$–0 emission integrated from 39 to 59 km s^{-1} with levels of 3, 4, 7, 10 and 13.5 K km s^{-1} (also indicated in the image). The rms noise of the ^{13}CO integrated emission is about 0.5 K km s^{-1}.

8 kpc (Churchwell et al. 2006), we can confirm the near distance for the bubbles N21 and N22. Hereafter we assume a distance of about 4 kpc for the whole complex.

In order to have a rough estimate of the mass of the molecular gas we use the ^{13}CO $J = 1$–0 emission and assume local thermodynamic equilibrium (LTE) to obtain the H$_2$ column density towards the molecular cloud shown in Fig. 3. We use:

$$N(^{13}CO) = 2.42 \times 10^{14} \frac{T_{ex} \int \tau_{13} dv}{1 - \exp(-5.29/T_{ex})} \quad (1)$$

to obtain the ^{13}CO column density, where T_{ex} is the excitation temperature and τ_{13} the optical depth. Assuming that the ^{13}CO $J = 1$–0 line is optically thin, we use the approximation

$$\int \tau_{13} dv \sim \frac{1}{J(T_{ex}) - J(T_{BG})} \int T_B dv \quad (2)$$

where

$$J(T) = \frac{5.29}{e^{5.29/T} - 1}, \quad (3)$$

$T_{BG} = 2.7$ K is the background temperature and T_B is the brightness temperature of the line. Following Anderson et al. (2009) we assume that T_{ex} is 20 K. The integration in equation (2) was done between 39 and 59 km s^{-1}. Using the relation $N(H_2)/N(^{13}CO) \sim 5 \times 10^5$ (e.g. Simon et al. 2001) we obtain an averaged column density of $N(H_2) \sim 7 \times 10^{21}$ cm^{-2} for the structure delimited by the 3 K km s^{-1} contour in Fig. 3. Finally, we estimate a mass of $\sim 10^5$ M$_\odot$ for the molecular cloud. This value was obtained from:

$$M = \mu m_H \sum_i \left[D^2\, \Omega_i\, N_i(H_2) \right], \quad (4)$$

where Ω is the solid angle subtended by the ^{13}CO $J = 1$–0 beam size, m_H is the hydrogen mass, μ is the mean molecular weight that is assumed to be 2.8 by taking into account a relative helium abundance of 25 per cent, and D is the distance assumed to be 4 kpc. Summation was performed over the whole molecular structure, i.e. over all the observed positions within the 3 K km s^{-1} contour level (see Fig. 3).

Additionally, we estimate the molecular density of the cloud densest portion, i.e. the area delimited by the 13.5 K km s^{-1} contour in Fig. 3. By considering an ellipsoid of semi-axis of 2 × 1 arcmin^2 centred at $l = 18°.146$, $b = −0°.308$, we obtain a mass of 5.5×10^3 M$_\odot$, which gives a density of about 9×10^3 cm^{-3}. The estimated mass of the whole molecular cloud and the density of its densest portion show that there is enough gas to probably form another generation of massive stars. Thus, we conclude that this region is a good scenario to test triggered star formation processes in further works.

4 LOOKING FOR OB-TYPE STARS

4.1 Optical observations

In order to look for sources responsible of ionizing the gas in the H II regions, we first search for OB-type in catalogues such as Reed (2003). Besides the stars suggested by Watson et al. (2008) to ionize the N21 bubble, we did not find any OB star catalogued towards the whole region displayed in Fig. 1. Thus, with the goal of finding the H II region exciting sources (or some of them) and possible nearby massive stars, we perform spectroscopic optical observations towards a sample of stars. We focus our attention on those stars lying inside a region defined by the external radius of each
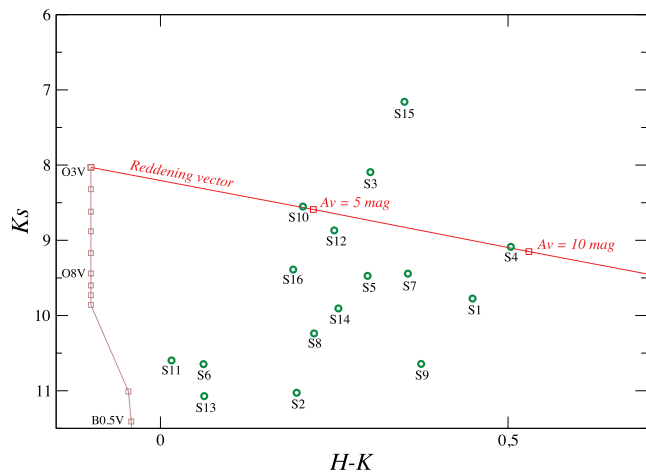
Figure 4. Colour–magnitude *Ks* versus (*H-Ks*) diagram of the selected OB star candidates towards the complex. The source numbers are the same as presented in Fig. 5. The squares along the vertical lines indicate the location of the no-reddened main-sequence stars between O3V and B0.5V using a distance of 4 kpc. The reddening slope for an O3V (Rieke & Lebofsky 1985) is shown with a red line with the squares placed at intervals corresponding to five magnitudes of visual extinction.

H II region, i.e. the external border delimited by the 8 μm emission. Then, we select the stars whose position in a typical near-IR colour–magnitude diagram [*Ks* versus (*H-Ks*)] suggests that they are OB-type stars. This diagram was constructed by using the magnitudes extracted from the two Micron All Sky Survey (2MASS) All-Sky Point Source Catalogue and by assuming a distance of about 4 kpc. Finally, we select those stars that can be observed in optical wavelengths with the 2.15 m telescope at CASLEO, Argentina, i.e. the optical counterparts of the 2MASS sources with a limit of $V = 15.6$ mag according to the Naval Observatory Merged Astrometric Data set (NOMAD; Zacharias et al. 2004). Fig. 4 shows the position of the selected sources in the near-IR colour–magnitude diagram, and Fig. 5 presents the physical position of these stars, successfully observed at CASLEO, over a two-colour image (8 μm = red, Hα = green). As can be seen in Fig. 4 all sources are located in the region of OB-type stars with exception of S15. However we decided to observe it in CASLEO because it lies at the centre of the possible unknown H II region.

4.1.1 Observations and data reduction

The optical observations were carried out in two runs in 2011 and 2012. The REOSC spectrograph attached to the 2.15 m telescope at CASLEO was used in simple dispersion. The spectra were taken with gratings of 300 and 600 grooves mm^{-1}, providing a dispersions of 3.4 and 1.6 Å pixel^{-1} with wavelength ranges of 3500–7000 Å and 5220–6830 Å, respectively. The slit was opened to 3.0 and 2.5 arcsec (consistent with the seeing at the site). The exposure time was 3600 s in all cases. The optical spectra were reduced and normalized using standard techniques with IRAF.[1]

In general, the obtained spectra have good signal-to-noise ratio (S/N) and few absorption lines were identified. They are useful to

---

[1] IRAF: the Image Reduction and Analysis Facility is distributed by the National Optical Astronomy Observatories, which is operated by the Association of Universities for Research in Astronomy, Inc. (AURA) under cooperative agreement with the National Science Foundation (NSF).
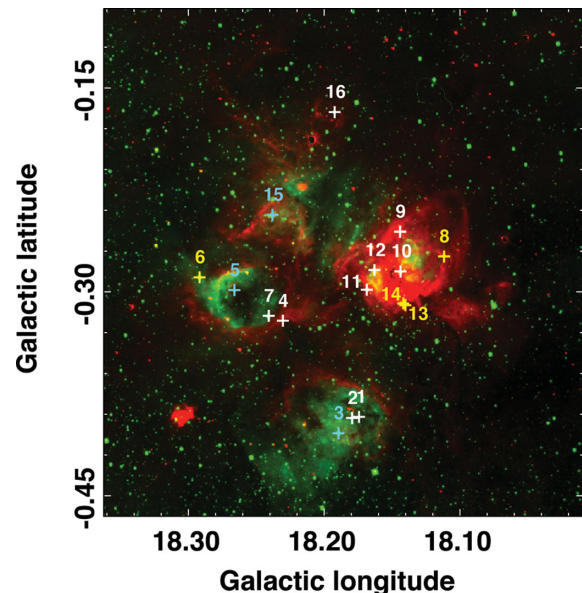
Figure 5. Two-colour image with the IRAC-*Spitzer* 8 μm emission displayed in red, and the Hα from the SuperCOSMOS H-alpha Survey (Parker et al. 2005) in green. The crosses show the position of the stars that were successfully observed with the 2.15 m telescope at CASLEO, Argentina. They are numbered according to Table 2. The discovered O and B-type stars are displayed in cyan and yellow, respectively.

perform a rough spectral type classification of the observed stars. At least, O and/or B-type stars can be distinguished from other spectral types, which is important to point the presence of massive and ionizing stars in the region.

4.1.2 Stellar content

Table 2 presents the observed stars with their 2MASS designation and JHKs photometry (Columns 1 to 5). In Columns 6 and 7 we include the main optical spectroscopic feature obtained from the spectral analysis and the Equivalent Width (EW) of the diffuse interstellar band (DIB) at 5893 Å, respectively. Finally, the S/N of the spectra is presented in Column 8. In Column 6, we remark if absorption lines of He I and He II are observed in the stellar spectrum, which is the most important feature for our analysis. Following Walborn & Fitzpatrick (1990) we can infer that the stars with He II absorption lines are O-type stars (S3, S5 and S15), while those sources with only He I absorption lines (sources S6, S8, S13 and S14) should be B0-5 stars. The spectra of these sources are shown in Fig. 6. Particularly interesting is the spectrum of source S15, which shows emission of N III, indicating a star of Population I or III (Walborn & Fitzpatrick 1990). From the I(4541)/I(4471) ratio we can infer that S15 may be an O8-9 star. In the case of source S9, the spectrum (not presented in Fig. 6) shows some hints of He I absorption lines, but it is not possible to confirm it due to the low S/N.

For sources S3, S5 and S15, the O-types stars, we estimated their radial velocities using the spectra obtained with the 600 grooves mm^{-1} grating. The radial velocities were estimated by averaging the values obtained from the He II and He I absorption lines (at wavelengths of 5411.52, 5875.62 and 6678.15 Å). The obtained velocities with respect to the local standard of rest are: $v_{LSR} \sim (53, 52$ and $32) \pm 23$ km s^{-1} for S3, S5 and S15, respectively. These velocities, within the large error bar, are roughly in agreement with

**Table 2.** NIR photometric and optical spectral information from the observed stars.

Star	2MASS designation	J (mag)	H (mag)	Ks (mag)	Main optical † feature	EW_{5893} (Å)	S/N
S1	18252783−1317114	11.224	10.223	9.774	−	−	15
S2	18252859−1316565	11.672	11.224	11.028	Balmer lines	−	30
S3	18253221−1316438	9.005	8.395	8.093	He II absorption lines	2.2	30
S4	18251888−1312139	10.739	9.592	9.088	No Balmer lines	1.5	40
S5	18251808−1309427	10.293	9.770	9.472	He II absorption lines	1.5	30
S6	18251894−1308045	10.811	10.709	10.647	He I absorption lines	0.2	50
S7	18251943−1311340	10.191	9.580	9.389	No Balmer lines	8.5	40
S8	18245470−1317125	10.990	10.459	10.238	He I absorption lines	1.0	70
S9	18245468−1314584	11.576	11.018	10.643	He I absorption lines (?)	0.8	20
S10*	18250115−1315490	9.460	8.757	8.552	Balmer lines	2.7	30
S11	18250674−1314526	10.847	10.613	10.597	Strong Balmer lines	1.2	170
S12	18250312−1314462	11.330	11.134	11.071	Strong Balmer lines	1.2	90
S13*	18250606−1316423	9.707	9.119	8.869	He I absorption lines	1.0	50
S14*	18250579−1316349	10.750	10.162	9.906	He I absorption lines	0.8	110
S15	18250290−1309385	8.046	7.509	7.158	He II absorption lines	2.3	30
S16*	18244104−1309573	10.253	9.799	9.443	Strong Balmer lines	−	70

Note. The * in the sources means that no nebular emission at Hα is detected near the star.

† He I absorption lines(?): the spectrum shows some hints of He I absorption lines.

No Balmer lines: Balmer lines are not detected, suggesting to be a late spectral type.
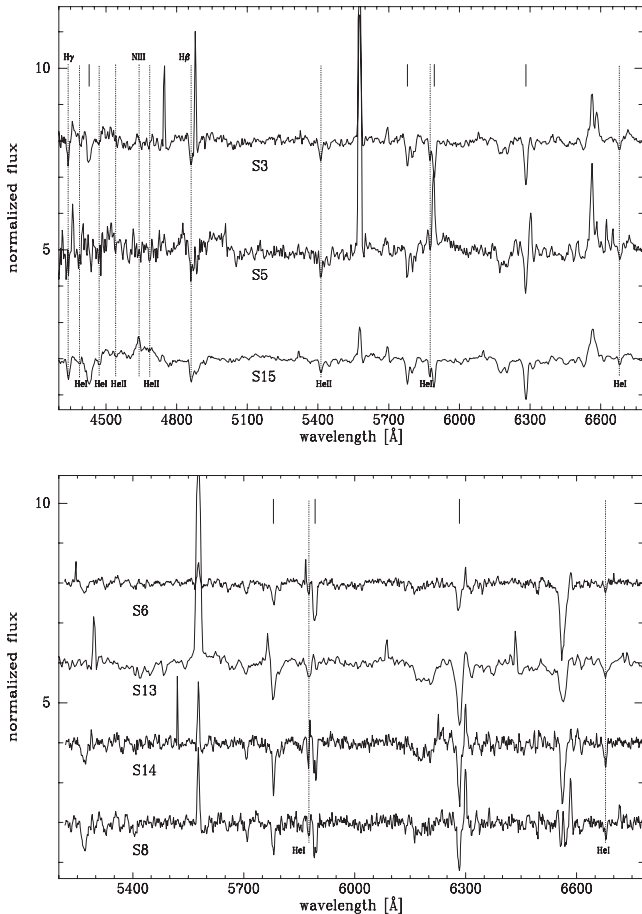
Figure 6. Optical low-resolution spectra of O and B stars, upper and lower panel, respectively. All detected stellar lines are indicated (dotted line), short solid lines indicate interstellar absorption.

the molecular gas velocity range and with the velocities of the H II regions (see Sections 2 and 3).

One important result is that we confirm the presence of a not catalogued H II region (the region indicated with an interrogation mark in Fig. 1), from which we very likely identified its exciting O-type star (source S15).

As mentioned above, Watson et al. (2008) suggested some stars to be the possible exciting sources of N21. Two of those stars are included in our sample: S1 and S3 (IN21-2 and IN21-1, respectively, in Watson et al. 2008). According to these authors, our source S3 (IN21-1 in their work) is the best candidate star for producing N21. They point out that spectroscopic observations suggest that it should be a late-O supergiant star, which is in agreement with our observations. In the case of source S1, we could not observe any significant stellar feature due to the low S/N, being impossible to conclude anything on this source.

4.2 X-ray point sources

Since first X-ray observations with the *Einstein*, *ROSAT* and *ASCA* satellites, it is well established that hot massive stars are intense X-ray emitters. We look for X-ray point sources in the *Chandra* Source Catalogue (Evans et al. 2010) towards the studied region. We found two sources: CXO J182438.1−131039 and CXO J182502.8−130933 (hereafter SX1 and SX2, respectively), which are shown in Fig. 7. It is important to note that source SX2 coincides with the above analysed source S15, a very likely O-type star which is exciting an uncatalogued H II region, while SX1 does not coincide with any source analysed at the optical wavelengths and lies in projection over the SNR shell close to the H II region G18.197−00.181.

These sources were observed in two observation runs. One was with the HRC on 2012 August 20 (Obs.Id. 9006). However, the total exposure of this observation was too short (∼1.1 ks) to perform a reliable analysis. The other observation run was obtained with the ACIS detector on 2012 June 19 (Obs.Id. 11883) with a total exposure time of 10.0 ks. The data were acquired in faint mode,
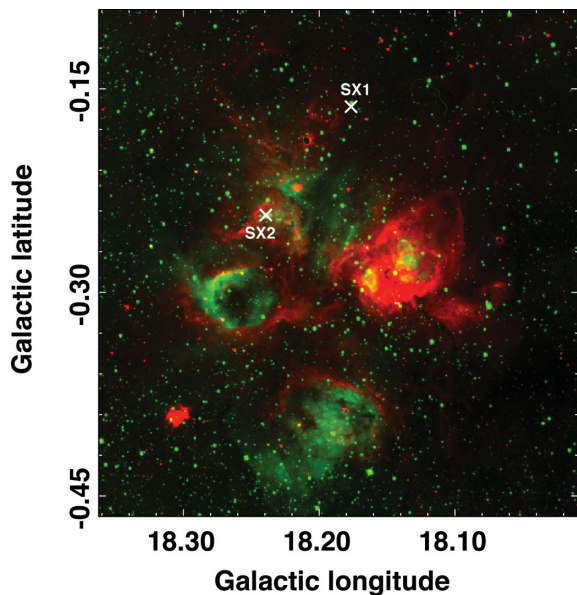
Figure 7. Same as Fig. 5 with the two X-ray point sources found in the *Chandra* Source Catalogue.

with six CCD turned on, two comprising the ACIS-I array [2,3], plus CCDs [5,6,7,8] of ACIS-S. However, the data from two CCDs of ACIS-I are not used in the followings because of the degraded point spread function and reduced effective area.

4.2.1 Analysis

To analyse the data and produce a level 2 event file, we processed the level 1 event list using the CIAO 4.4 and CALDB 4.5.3 set of calibration file. We retain events with grades = 0, 2, 3, 4, 6 and status = 0, and assume a constant background flux due to the lack of flaring background events. To improve the sensitivity to faint sources, we filtered out events outside [500:8000] eV band. We generated a source image and a congruent exposure map (assuming a monochromatic spectrum, $kT = 2.0$ keV) following standard CIAO threads.[2]

Unfortunately, in the observation Id. 11883 the source SX2 lies at the gap between ACIS-I and ACIS-S chips. However, we used the short observation Id. 9006 in order to estimate an upper limit X-ray emission level for this source. We were able to detect SX1 as an X-ray source with a total of ∼ 80 photons, and for SX2, we obtained a very marginal detection with a total of five background corrected photons.

It can be noticed that we do not observe diffuse emission from the SNR G18.1−0.1. As mentioned above, this SNR was previously detected in X-rays with the *ASCA* satellite in the 0.7–10 keV energy range (Sugizaki et al. 2001). These authors converted X-ray photons to energies using a single absorbed power-law model to obtain a flux of 5.4×10^{-13} erg cm^{-2} s^{-1}. However, taking into account the *ASCA* low spatial resolution (40 arcmin) and the SNR size (8 arcmin), this flux must be spanned over this area. By rescaling this flux at the *Chandra* spatial resolution we computed the diffuse X-ray emission level of the SNR. We used the PIMMS[3] software to obtain an upper limit flux density of about 1.9×10^{-14} erg cm^{-2} s^{-1} arcmin^{-2}, which is below the detection threshold of this ACIS-S observation.

[2] http://asc.harvard.edu/ciao/threads/expmap_acis_single/
[3] http://heasarc.gsfc.nasa.gov/Tools/w3pimms.html

Table 3. X-ray parameters of source SX1.

Parameter	SX1
$N_{\rm H}$ (cm^{-2})	$1.82(\pm 0.32) \times 10^{22}$
kT (keV)	0.59 ± 0.12
Abundance	1.62 ± 0.93
Norm.	$2.5(\pm 1.48) \times 10^{-4}$
Flux (cgs)	3.94×10^{-14}
Unabsorbed flux (cgs)	1.18×10^{-12}
$L_{\rm x}$ (erg s^{-1})	2.25×10^{33}

To characterize the hot plasma responsible of the X-ray emission of source SX1, and to estimate the intrinsic X-ray luminosity, we analysed the ACIS-S spectra. We extracted source photons by using a circular region of radii 2.9 arcmin. A total of 87 X-ray photons were acquired from source SX1 for a total of 10 ks with a median energy of 1.53 keV. The spectral fitting model consists of a combination of absorption and emission models. Absorption WABS model was used to account for the action of the circumstellar medium, while we assumed emission by a thermal plasma, in collisional ionization equilibrium, as modelled by the APEC code (Smith et al. 2001). Elemental abundances are not easily constrained with low-statistic spectra, but it was left free during the fitting procedure. Spectral parameters are shown in Table 3, while Fig. 8 shows the observed SX1 spectrum and the fitted solution. It is clear that some spectral emission lines appear blended, being the most intense from Si XIII (1.864 keV).

In the 0.5–8.0 keV range, we calculated an X-ray flux of 3.94×10^{-14} erg cm^{-2} s^{-1} for SX1, while the corrected absorbed X-ray flux is 1.18×10^{-12} erg cm^{-2} s^{-1}. Assuming a distance of 4 kpc, the unabsorbed X-ray luminosity is $L_{\rm x} \sim 2.25 \times 10^{33}$ erg s^{-1}, which is a typical emission level of an early O-type star (O3-O5). Optical spectra recently obtained by Halpern (private communication) confirms this. The estimated upper limit X-ray emission level for source SX2 suggests that it also could be an O-type star; however longer exposure observations are needed in order to confirm it. In conclusion, the X-ray analysis strongly suggests the presence of other early O-type star in the region (SX1) and encourages to obtain longer X-ray observations
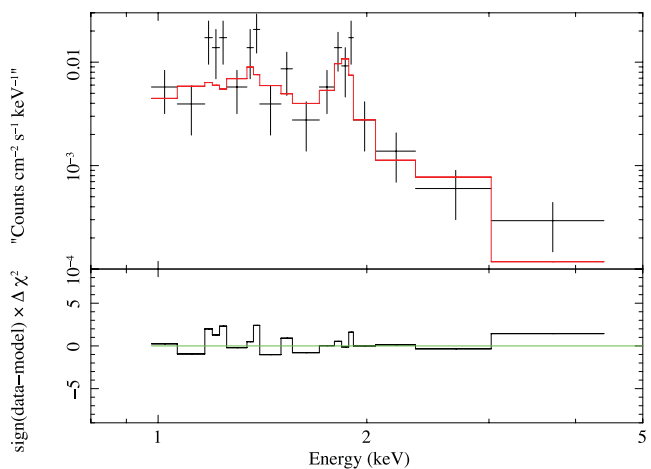
Figure 8. X-ray spectrum obtained towards source SX1. The spectrum was binned to reach a minimum of four and nine counts per channel. The red line shows the best-fitting model. The broad observed emission lines (line blending effect) are produced due to the low resolution of the spectra. The reduced chi-square is 1.05 for 16 degree of freedom.
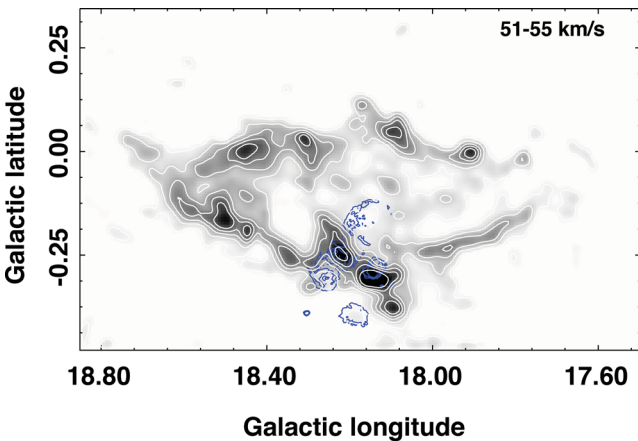
towards the region in order to study, in the high energy regime, the OB-type stars content.

5 THE H II REGION/SNR COMPLEX SURROUNDINGS: THE BIG PICTURE

In this section, we analyse the H II region/SNR complex surroundings in a larger spatial scale. A detailed inspection of the whole ^{13}CO data cube at larger scale reveals that the H II region/SNR complex lies in a border of a big molecular shell that peaks in the velocity interval of 51–55 km s^{-1}. By inspecting the mid-IR emission in this large-scale area we did not find any possible counterpart to this molecular shell. Fig. 9 presents the ^{13}CO $J = 1$–0 emission of a large region of about $1°.3 \times 0°.8$ integrated between 51 and 55 km s^{-1}. It is important to note that the H II region/SNR complex is located southwards a very likely molecular shell with an elliptical shape with semi-axes of 30×12 arcmin^2, centred at $l = 18°.185$, and $b = -0°.104$. Assuming a distance of 4 kpc, the molecular shell has an extension of about 70 pc $\times$ 28 pc. Following the standard nomenclature for Galactic shells, we designate this new structure as GSH 18.2−0.1+53. Along the mentioned velocity range, the CO shell is well defined as a large structure, although, as in many other shells, the typical behaviour of an expanding structure (i.e. a ring that starts as a cap, reaches its greatest angular dimension at the systemic velocity and then shrinks back to a cap) is not completely observed. Fig. 9 also shows that the shell is composed of several molecular condensations among which are those associated with the H II region/SNR complex.

Following the same assumptions and equations as in Section 3 we derive an average H$_2$ column density for the whole molecular shell. Assuming a constant $T_{ex} = 20$ K over the shell and a $\Delta v = 4$ km s^{-1}, we obtain $N(H_2) \sim 5 \times 10^{21}$ cm^{-2}. Using equation (4) and performing the summation over all the observed positions within the 1.2 K km s^{-1} contour level (which define the shell boundary; see Fig. 9) we obtain a total molecular mass of about 2×10^5 M$_\odot$. Following Weaver et al. (1977), we estimate the kinetic energy stored in the shell and its age using $E_{kin} = 0.55 \times M_{shell} \times V_{exp}^2$ and $t_{dyn} = 0.6 R_{eff}/V_{exp}$, respectively, in which is considered a simple model that describes the expansion of a shell created by a continuous injection of mechanical energy, where R_{eff} is the effective radius. Table 4 summarizes the main physical parameters of GSH 18.2−0.1+53.

The origin of most of these expanding structures would be related to the action of massive stars (OB-type stars) and their descendants (WR stars), which strongly disturb the environment that surrounds them, first by the high rate of ionizing photons and strong winds, and subsequently at the end of their lives, when they explode as supernovae. In this context, we wonder for the origin of GSH 18.2−0.1+53. We have not found any OB star catalogued towards the interior of the shell. But of course we cannot discard that this shell has been originated by the action of massive stars. Our X-ray analysis strongly suggests that SX1, which lies in the interior of the molecular shell, is an O-type star, probably one of those which are responsible, together with other undetected OB-type stars and even the SNR progenitor, for generating the shell. Regarding an SNR origin we consider two possible scenarios: (i) the contribution of the SNR G18.1−0.1, and (ii) the action of an ancient SNR not observed at the present day. Given that the effective action of SNR G18.1−0.1 is limited to the borders defined by the radio continuum shell, and considering that typical ages for SNRs are at most 10^5 yr, we discard that G18.1−0.1 has originated the big shell by itself. However, as mentioned above, its massive progenitor could have contributed to generate it. By the other hand, considering the scenario where the origin of GSH 18.2−0.1+53 is attributed to an ancient SNR that would have injected to the ISM a mechanical energy of about 10^{51} erg, from which the shell still preserves about 1 per cent of that energy, it could be a similar case as was proposed for the surroundings of the SNR G349.7+0.2 (Reynoso & Mangum 2001). In that case it was found that the SNR, some *IRAS* sources and an UCHII region lie in a border of an extended molecular shell, suggested to be the fossil remains of an ancient SN explosion. Summarizing, the origin of GSH 18.2−0.1+53 still remains uncertain and it deserves a deeper study, e.g. new observations towards its interior in order to look for OB-type stars.

6 SUMMARY

The SNR G18.1−0.1 is located, along the plane of the sky, close to several H II regions (infrared dust bubbles N21 and N22, and the H II regions G018.149−00.283 and G18.197−00.181). Taking into account the catalogued distances and/or systemic velocities of these structures, and our analysis of the molecular gas related to them, we suggest that all of these objects belong to a same complex at a distance of about 4 kpc. This could be a clear observational evidence supporting that massive stars are born predominantly within dense cores of giant molecular clouds and evolve in clusters, which can generate several neighbouring H II regions and SNRs. The main results of this work can be summarized as follows.

Figure 9. Large-scale ISM: ^{13}CO $J = 1$–0 emission integrated between 51 and 55 km s^{-1} with white contours of levels of 1.2, 1.8, 3.0, 4.0, 5.8 and 7.5 K km s^{-1}. The blue contours correspond to the radio continuum emission at 20 cm, showing the SNR and the H II regions positions.

Table 4. Main physical parameters of the big molecular shell.

R_{eff} (pc)	V_{sys} (km s^{-1})	$V_{exp} = \Delta v/2$ (km s^{-1})	Mass ($\times 10^5$ M$_\odot$)	E_{kin} $\times 10^{48}$ (erg)	t_{dyn} (Myr)
24.5 ± 1.3	53.1 ± 0.2	2.0 ± 0.2	2.0 ± 1.1	9.0 ± 0.6	7.0 ± 2.7

(1) Analysing the ^{13}CO $J = 1$–0 emission towards the H II region/SNR complex we found several molecular structures very likely related to the sources within the velocity range between 39 and 59 km s^{-1}. The molecular gas morphology suggests that it is very likely being swept and shaped by the expansion of the H II regions, mainly by the infrared dust bubbles N21 and N22, and the H II region G018.149−00.283. We obtained a molecular mass for the whole structure related to the complex of about 10^5 M$_\odot$. We estimated a density of about 9×10^3 cm^{-3} for the densest portion of this molecular structure.

(2) Using spectroscopic optical observations obtained with the 2.15 m telescope at CASLEO, Argentina, we searched for OB-type stars in order to look for sources responsible of ionizing the gas in the H II regions. We discovered three O-type stars very likely exciting the bubbles N21 and N22, and an uncatalogued H II region northward of bubble N22, respectively. Thus, we confirm the presence of an unknown H II region. Additionally, we discovered four B0-5 stars, one towards the bubble N22 and the others within the H II region G018.149−00.283.

(3) Taking into account that hot massive stars usually are X-ray emitters, we looked for X-ray point sources in the *Chandra* Source Catalogue. We found two sources, one of them coincides with the above mentioned star that is exciting the uncatalogued H II region. Estimating an upper limit for its X-ray emission level we can only suggest that it may be an O-type star. On the other side, the X-ray analysis of the other source, which lies over the SNR shell, strongly suggests that it is an early O-type star (O3-O5).

(4) By inspecting the ISM surrounding the H II region/SNR complex in a large scale, we discovered a big molecular shell peaking between 51 and 55 km s^{-1}. Assuming a distance of 4 kpc, this shell has an extension of about 70 pc $\times$ 28 pc, and the analysed H II region/SNR complex appears to be located in its southern border.

ACKNOWLEDGEMENTS

REFERENCES

Anderson L. D., Bania T. M., 2009, ApJ, 690, 706
Anderson L. D., Bania T. M., Jackson J. M., Clemens D. P., Heyer M., Simon R., Shah R. Y., Rathborne J. M., 2009, ApJS, 181, 255
Benjamin R. A. et al., 2003, PASP, 115, 953
Brand J., Massi F., Zavagno A., Deharveng L., Lefloch B., 2011, A&A, 527, A62
Brogan C. L., Gelfand J. D., Gaensler B. M., Kassim N. E., Lazio T. J. W., 2006, ApJ, 639, L25
Carey S. J. et al., 2009, PASP, 121, 76
Churchwell E. et al., 2006, ApJ, 649, 759
Churchwell E. et al., 2007, ApJ, 670, 428
Deharveng L., Zavagno A., Caplan J., 2005, A&A, 433, 565
Downes D., Wilson T. L., Bieging J., Wink J., 1980, A&AS, 40, 379
Elmegreen B. G., Lada C. J., 1977, ApJ, 214, 725
Evans I. N. et al., 2010, ApJS, 189, 37
Everett J. E., Churchwell E., 2010, ApJ, 713, 592
Fich M., Blitz L., Stark A. A., 1989, ApJ, 342, 272
Green D. A., 2009, BASI, 37, 45
Helfand D. J., Becker R. H., White R. L., Fallon A., Tuttle S., 2006, AJ, 131, 2525
Jackson J. M. et al., 2006, ApJS, 163, 145
Ji W.-G., Zhou J.-J., Esimbek J., Wu Y.-F., Wu G., Tang X.-D., 2012, A&A, 544, A39
Kolpak M. A., Jackson J. M., Bania T. M., Clemens D. P., Dickey J. M., 2003, ApJ, 582, 756
Lefloch B., Lazareff B., 1994, A&A, 289, 559
Lefloch B., Lazareff B., 1995, A&A, 301, 522
Lockman F. J., 1989, ApJS, 71, 469
McKee C. F., Ostriker E. C., 2007, ARA&A, 45, 565
Nicholas B., Rowell G., Burton M. G., Walsh A., Fukui Y., Kawamura A., Longmore S., Keto E., 2011, MNRAS, 411, 1367
Odegard N., 1986, AJ, 92, 1372
Ortega M. E., Paron S., Cichowolski S., Rubio M., Castelletti G., Dubner G., 2010, A&A, 510, A96
Parker Q. A. et al., 2005, MNRAS, 362, 689
Paron S., Ortega M. E., Rubio M., Dubner G., 2009, A&A, 498, 445
Petriella A., Giacani E., Paron S., 2011, Boletin de la Asociacion Argentina de Astronomia, 54, 235
Petriella A., Paron S. A., Giacani E. B., 2012, A&A, 538, A14
Pomarès M. et al., 2009, A&A, 494, 987
Povich M. S. et al., 2007, ApJ, 660, 346
Reed B. C., 2003, AJ, 125, 2531
Reynoso E. M., Mangum J. G., 2001, AJ, 121, 347
Rieke G. H., Lebofsky M. J., 1985, ApJ, 288, 618
Sharpless S., 1959, ApJS, 4, 257
Simon R., Jackson J. M., Clemens D. P., Bania T. M., Heyer M. H., 2001, ApJ, 551, 747
Smith R. K., Brickhouse N. S., Liedahl D. A., Raymond J. C., 2001, ApJ, 556, L91
Sugizaki M., Mitsuda K., Kaneda H., Matsuzaki K., Yamauchi S., Koyama K., 2001, ApJS, 134, 77
Walborn N. R., Fitzpatrick E. L., 1990, PASP, 102, 379
Watson C. et al., 2008, ApJ, 681, 1341
Weaver R., McCray R., Castor J., Shapiro P., Moore R., 1977, ApJ, 218, 377
Zacharias N., Monet D. G., Levine S. E., Urban S. E., Gaume R., Wycoff G. L., 2004, BAAS, 36, 1418

This paper has been typeset from a TEX/LATEX file prepared by the author.